Published in final edited form as:

Cancer Chemother Pharmacol. 2015 April ; 75(4): 671–682. doi:10.1007/s00280-015-2675-1.

Comparative Pharmacokinetic Properties and Antitumor Activity of the Marine HDACi Largazole and Largazole Peptide Isostere

John L. Pilon[a], **Dane J. Clausen**[d], **Ryan J. Hansen**[b], **Paul J. Lunghofer**[b], **Brad Charles**[b], **Barbara J. Rose**[b], **Douglas H. Thamm**[b,e], **Daniel L. Gustafson**[b,e], **James E. Bradner**[c], and **Robert M. Williams**[d,e,*]

[a]Cetya Therapeutics, 1301 Center Avenue, Fort Collins, CO 80523

[b]Flint Animal Cancer Center, Colorado State University, 300 West Drake Road, Fort Collins, CO 80523

[c]Department of Medical Oncology, Dana-Farber Cancer Institute, Boston, MA 02115

[d]Department of Chemistry, Colorado State University, 1301 Center Avenue, Fort Collins, CO 80523

[e]University of Colorado Cancer Center, Aurora, Colorado 80045

Abstract

Purpose—Largazole is a potent class I selective HDACi natural product isolated from the marine cyanobacteria *Symploca sp*. The purpose of this study was to test synthetic analogs of Largazole to identify potential scaffold structural modifications that would improve the drug-like properties of this clinically relevant natural product.

Methods—The impact of Largazole scaffold replacements on *in vitro* growth inhibition, cell cycle arrest, induction of apoptosis, pharmacokinetic properties, and *in vivo* activity using a xenograft model were investigated.

Results—*In vitro* studies in colon, lung, and pancreatic cancer cell lines showed that pyridyl substituted Largazole analogs had low nanomolar/high-picomolar activity on cell proliferation, and induced apoptosis and cell cycle arrest at concentrations equivalent to or lower than the parent compound Largazole. Using IV bolus delivery at 5mg/kg, two compartmental pharmacokinetic modeling on the peptide isostere analog of Largazole indicated improved pharmacokinetics including AUC, CL, and Vss. In the A549 non-small cell lung carcinoma xenograft model using a dosage of 5 mg/kg administered intraperitoneally every other day, Largazole, Largazole thiol, and Largazole peptide isostere demonstrated tumor growth inhibition (TGI%) of 32, 44, and 66 percent respectively. Moreover, the decreased tumor growth rate for Largazole peptide isostere was statistically significant compared to control (p=0.002) and superior to Largazole (p=0.006). Surprisingly tumor growth inhibition in this system and treatment regimen was not observed with the potent pyridyl-based analogs.

Corresponding author contact information: Robert M. Williams, rmw@lamar.colostate.edu; Tel.: 1-970-491-6747; FAX: 1-970-491-3944.

Conflict of Interest Statement: JLP and RMW are co-founders of Cetya Therapeutics, Inc.

Conclusions—Our results establish that replacing the depsipepitde linkage in Largazole with an amide may impart pharmacokinetic advantage and that alternative prodrug forms of largazole are feasible.

Keywords

Largazole; histone deacetylase inhibitor; peptide isostere; prodrug; depsipeptide

Introduction

The interest in histone deacetylase inhibitors (HDACi) as therapeutic agents in oncology has grown rapidly over the previous ten years. Hundreds of clinical trials have been conducted with HDACi, primarily in oncological settings as a single agent or in combination therapy with more established therapeutic regimens. The successes of HDACi in clinical trials has been varied with some studies showing little benefit to the patient, while the HDACi Istodax (Romipdepsin, FK228) was shown to be quite efficacious and worthy of FDA approval for cutaneous T-cell lymphoma (CTCL) and peripheral T-cell lymphoma (PTCL)(1–3).

HDACi can be structurally classified broadly into five classes; hydroxamates, benzamides, cyclic peptides, shorty chain fatty acids, and the recently characterized trifluoromethyloxadiazole's (TFMO) (4,5). The vast majority of clinical development to date has focused on hydroxamate class HDACi. The hydroxmates are highlighted by the FDA approved Zolinza (Vorinostat, SAHA) and the clinically advanced Panobinostat (LBH-589) currently in phase III development in combination with Bortezomib-Dexamethasone in patients with relapsed multiple myeloma (6–8). Hydroxmates exhibit broad inhibitory profiles and are considered pan-HDACi inhibiting class I and class IIa/b HDACs at therapeutic levels. Recently however, the concept of pan-HDACi has been thrown into question and the frequently reported high inhibitory activity to Class IIa HDACs is likely an artifact of commonly used substrates used to determine potency (9). Benzamide class HDACi are generally more selective and only inhibit class I HDACs at therapeutic levels, but are generally less potent than hydroxamate HDACi (10). The most clinically relevant and advanced benzamide is Entinostat (MS-275) currently entering phase III development for estrogen receptor-positive advanced breast cancer in combination with Exemestane. The TFMO class is a new addition to the HDACi family of compounds with an inhibitory profile that is reportedly restricted to class IIa HDACs, the first inhibitors convincingly shown to target this class of deacetylases. The final two classes of HDACi are the short chain fatty acids such as butyrate and valproate and the cyclic depsipeptide class of HDACi. The cyclic depsipeptide HDACi consist largely of natural products including Rompidepsin (FK228), Spiruchostatins, and the recently discovered marine HDACi, Largazole.

Largazole, isolated via bioactive fractionation from the marine cyanobacteria species *Symploca* by Leusch and colleagues, was shown to have excellent antineoplastic activity (11). Subsequent work by Luesch and others revealed that the new compound was indeed a potent class I-selective HDACi, leading to a flurry of synthetic activity on this potentially clinically important natural product (12–14). Largazole contains a 3-hydroxy-7-

mercaptohept-4-enoic acid moiety common to several other macrocyclic depsipeptide natural products including FK228 (Romidepsin), FR901375, and the Spiruchostatins. As with the other depsipeptide-based HDACi's, Largazole is a prodrug requiring *in vivo* cleavage of the octanoyl residue to reveal the active thiol from of the compound that acts to chelate the Zn^{2+} ion found in the active site of the zinc-dependent HDACs. Significantly, unlike Romidepsin where the prodrug is activated via reduction of a disulfide, the prodrug form of Largazole is liberated via facile lipase/esterase cleavage of the thioester. A second unique feature of Largazole is the macrocycle capping group that contains a thiazoline-thiazole unit that imparts excellent binding geometry for class I HDAC recognition (15).

In the present study, we have utilized novel macrocycle scaffold replacements of the parent compound Largazole and a pyridyl disulfide-based prodrug compound to investigate the potential to produce a lead-optimized HDACi that would improve pharmacokinetics and *in vivo* and *in vitro* performance. Compounds included in this study are the previously reported synthetic Largazole analogs that have undergone isosteric oxygen to nitrogen replacement to insert a peptide linkage in place of the depsipeptide pyridyl-thiazole substitutions and an alternative prodrug form (16,17).

Materials and Methods

Cell Culture and Growth Inhibition Assays

All cells were purchased from the American Type Culture Collection (Manassas, VA) and cultured in Dulbecco's modified Eagle medium (DMEM) (Lonza, Walkersville, MD) supplemented with 10% fetal bovine serum (Atlas Biologicals, Fort Collins, CO) and supplemented with amino acids (nonessential amino acids Cellgro/Corning Manassas VA) and maintained at sub-confluent densities at 37°C, humidified air and 5% CO_2. Cells were seeded in 96-well clear bottom NUNC plates at 3.0×10^3 (A549, HTC-116, HT-29) 6.0×10^3 (SW620) and 2.0×10^3 (MiaPaCa), and allowed to adhere overnight (16 hours). Media was replaced just prior to addition of Largazole or Largazole analogs prepared as 2 mM stocks in DMSO. Dilutions of stocks were made to cover the range of 40 M-4 pM. Cells were incubated in the presence of drug for 48 hours. After 48 hours, 10 L/well of sterile Resauzrin (Sigma Aldrich St. Louis MO) was added (200 g/mL in PBS) and incubated at 37°C for two-three hours followed by fluorescence measurements at (530ex/590em) on a Synergy HT plate reader (Biotek, Winooski, VT). Relative viable cell number was standardized to untreated cells and cell viability was assessed by calculating IC_{50} by entering the data into Prism GraphPad (La Jolla, CA) and performing three-parameter non-linear curve fitting to the data. All values are the average of at least three independent experiments.

HDAC Panel Inhibition

The method used for determination of IC50's to specific HDAC proteins is as reported in (12). In brief, purified full-length HDAC proteins HDAC1, HDAC2, HDAC3/NCor2 and HDAC6 0.6 (BPS Biosciences) was incubated with a commercially available fluorophore-conjugated substrate at a concentration equivalent to the substrate Km (Upstate 17-372; 6 μMfor HDAC1, 3 μM for HDAC2, 6 μM for HDAC3/NCoR2, and 20 μM for HDAC6).

Apoptosis by Annexin V/Propidium Iodide

Cells were plated in 6 well plates at a density of 2.5×10^5 per well in 2 mL DMEM in 10% fetal bovine serum and allowed to adhere to the plate overnight. Media was aspirated and cell monolayer was washed once with PBS containing penicillin and streptomycin (0.1%) and fresh DMEM was added to wells. Largazole or Largazole analogs were added at the concentrations indicated in the corresponding figure and cells were incubated for 24 hours. Media was collected into 15 mL conical tubes and wells washed once with PBS. Adherent cells were harvested by typsin/EDTA digestion and added to the tube. All cells were then pelleted via centrifugation at 1,200×g. Cell pellets were washed two times with PBS and re-suspended in 100 L 1× binding buffer and 2.5 L of annexin V (V450, BD Pharmingen™, San Jose CA). Cells were incubated at room temperature for 15 minutes in the absence of light and 1× binding buffer was added to a final volume of 400 L followed by the addition of 5 L of propidium iodide (50 g/mL in PBS, Sigma Aldrich, St. Louis, MO). Cells were analyzed in less than 1 hour on a CyAn ADP (Dako, Carpinteria, CA) flow cytometer along with the unstained and single stained cells to determine appropriate gating. All data was analyzed by FlowJo software (Ashland, OR). Micrograph images of the time-course experiment were acquired under at 10×magnification using the EVOS® Cell Imaging System (LifeTech, Carlsbad, CA)

Cell Cycle Distribution

Asynchronous cells were plated as above and collected as described for the annexin V assay above. Cells were fixed by adding drop-wise 1 mL of ice cold 70% ethanol and stored at −20° C until assay. Cells were pelleted, washed with once with PBS. Cell pellets were re-suspended in L PBS and 200 L extraction buffer (0.2 M Na_2HPO_4, 0.1M Citrate) followed by the addition of 500 L of propidium iodide (125 Worthington units/mL RNAase A and 50 g/mL propidium iodide, Sigma). The cell suspension was incubated at 37°C for 30 minutes followed by data collection via flow cytometry as above and analysis by FlowJo software using the Dean-Jett-Fox algorithm.

Western Blot

Cells were plated in six well plates and allowed to adhere overnight. The next day largazole and largazole analogs were added to the indicated concentrations and incubated for 24 h. Cells were lysed in 1×M-PER buffer (Pierce Chemical, Rockford, IL) containing HALT protease inhibitor cocktail (Pierce) and 0.1 mM phenylmethylsulfonyl floride, benzonase (EMD Millipore) was added to samples as needed to digest nucleic acid. The protein concentration was measured with the BCA Protein Assay kit (Pierce). Lysates containing equal amounts of protein were separated on NuPage bis-tris precast gels 4–12% (Life Technologies, Grand Island, NY), transferred to polyvinylidene difluoride membranes, blocked with SuperBlock (Pierce), and probed with antibodies. Antiacetyl histone H3 and H4 antibodies were purchased from Millipore (Ac-H3, 06-599; Ac-H4, 06-598). Primary antibodies were diluted 1/1000 in 5 mL SuperBlock and incubated with membranes containing transferred proteins over night with gentle agitation at 4°C. After incubation with primary antibody blots were washed 3×5 minutes in tris-buffered saline plus tween 20 (TBST). The secondary antibody (goat anti rabbit HRP conjugated, Pierce) was diluted

1/20,000 in SuperBlock and incubated at 4°C with gentle agitation for at least two hours followed by TBST wash as above. Detection of signal was performed with the SuperSignal Pico West Substrate (Pierce) per manufacturers instructions and image was acquired using a Molecular Imager® system equipped with a CCD camera (BioRad, Redman WA). Tumor lysates were generated as above with the exception that 50–100 mg of tumor tissue was placed into tubes and lysates were generated using a Bullet Blender® (Next Advance, Inc. Averill Park, NY).

K9 Ki-67 Automated IHC

Immunohistochemical staining were performed using standard techniques on an automated stainer (Autostainer Link 48; Dako; Carpenteria, CA). Briefly, 4-μm sections were cut and mounted on positively charged slides. The sections were deparaffinized and then rehydrated with descending alcohol concentrations to buffer. Heat-induced epitope retrieval with EDTA buffer (pH 8.0) for 20 minutes was followed by endogenous peroxidase blocking with 3% hydrogen peroxide and incubation with the primary antibody at room temperature for 30 minutes. The primary antibody used was a monoclonal mouse anti-human antibody at a dilution of 1:50 (M7240; Dako; Carpenteria, CA). A prediluted, universal secondary antibody and DAB based detection kit (K8023; Dako; Carpenteria, CA) were utilized to detect the immunoreactive complexes. The slides then were counterstained with Mayer's hematoxylin. Images for IHC analysis were acquired at 20×magnification using an Olympus BX40 microscope (Tokyo, Japan), a ProgRes Speed XT Core5 camera equipped with ProgRes Capture Pro 2.7 software (Jenoptik, Germany)

Animals, A549 Xenograft, Pharmcodynamic Dosing and IV Bolus Pharmacokinetic Analysis

All mice were housed 5 animals/cage in a controlled low-pathogen controlled environment. All animal handling was done to minimize pain, suffering, and distress as defined by the procedures and policies of Colorado State University animal handling and as detailed in the approved IACUC protocol 12-3592A. Female athymic NCr-*nu/nu* nude mice 6–8 weeks of age were purchased from NCI (Fredrick, MD) and acclimated. Tumors were established by subcutaneous injection of 1×10^7 A549 cells on the left rear flank in 100 L serum free DMEM mixed 1:1 with Matrigel (BD Biosciences, San Jose, CA). Tumor dimensions were measured every other day using a Vernier caliper. Tumor volumes were calculated by using the formula 0.5 ($W^2\times L$) where W = width and L = length (L) with the length being taken as the longest tumor dimension and tumor growth inhibition was determined by (TVcontrol day x- TVinitial) – (TVtreatment day x) /(TVcontrol day x- TVinitial), where TV is the respective tumor volume of control, treatment or initial measurement. Animals were sacrificed when tumor volumes reached ≥ 1000 mm^3. Tumor volumes and overall days to endpoint were entered into Prism and statistical significance was determined by pairwise Mann-Whitney T-test and Kaplan-Meier analysis. All compounds were prepared fresh on the day of treatment in DMSO and mice were treated via intraperitoneal injection every other day for 13 days at 5 mg/kg.

To show pharmacodynamic response to compound treatment animals that were at or near endpoint at day 35 of the study (last study day) were treated for 4 consecutive days with 5

mg/kg of test-articles as above. On day four animals were sacrificed and organs and tumors were collected. Tumors were sectioned and placed either into formalin for immunohistochemistry or snap frozen for western blot analysis.

For pharmacokinetic analysis, female NIH Swiss mice were dosed with 5 mg/kg largazole or largazole peptide isostere were prepared in 75:25 (DMSO:USP sterile saline for injection) and dosed via tail vein in a volume of 50 L per 25 g and euthanized at the indicated time points (*n*=3 per time point). Whole blood was collected by centrifugation after cardiac venipuncture into heparinized syringes. Whole blood was collected from mice of similar age and strain and used to make a standard curve ranging from 0 to 20,000 ng/ml along with quality control (QC) samples for determination of precision and accuracy. Samples (50 L) were spiked with 5 L internal standard (trazodone at 250 pg/ml) followed with the addition of 5 L of 75 mM dithiothreitol (DDT solution was prepared by first dissolving in Milli-Q water, then 1 ml of 0.1 N NaOH was added and finally 3.75 mL of 70/30 EtOH/Milli-Q was added). Samples were vortex mixed for 10 min, centrifuged for 5 min at 18,000×*g*. After allowing samples to stand for 15 minutes, 1 mL of ethyl acetate was added, vortex mixed for 10 min and again centrifuged for 10 min at 18,000×*g*. Nine hundred (900) microliters of the organic layer was transferred to empty 2 mL micro-centrifuge tubes and were placed in speed-vac (Savant AES 1000-120, Thermo Scientific, Asheville, NC) for approximately 1 hr. Samples were reconstituted in 100 L of 80/20: acetonitrile with 0.1% acetic acid/10 mM ammonium acetate with 0.1% acetic acid in Milli-Q, vortexed for 10 min and centrifuged for 5 min at 18,000×*g*. Samples were transferred to HPLC vials and analyzed by mass spectrometry.

Mass spectrometry

Positive ion electrospray ionization (ESI) mass spectra were obtained with a MDS Sciex 3200 Q-TRAP triple quadrupole mass spectrometer (Applied Biosystems, Inc., Foster City, CA) with a turbo ionspray source interfaced to a Shimadzu HPLC system (Columbia, MD). Samples were chromatographed with an XBridge Phenyl, 5 μm, 4.6×50 mm column (Waters Corporation, Milford, MA) protected by a C18 guard cartridge, 4.0×2.0 mm (Phenomenex, Torrance, CA). An LC gradient was employed with mobile phase A consisting of 10 mM ammonium acetate with 0.1% acetic acid and mobile phase B consisting of acetonitrile with 0.1% acetic acid. Chromatographic resolution was achieved by increasing mobile phase B linearly from 30% to 98% from 1 to 3 min, maintaining at 98% from 3 to 5 min, decreasing linearly from 98% to 30% from 5 to 6 min, followed by re-equilibration of the column at 30% mobile phase B from 6 to 7 min. The LC flow rate was 1 mL/min, the sample injection volume was 20 μL, and the analysis run time was 7 min.

The optimized mass spectrometer settings for Largazole and Largazole thiol are provided in Table 1. The source conditions were optimized as follows: turbo ionspray temperature, 550 °C; ion spray voltage, 1250 V; curtain gas, N_2, (CUR), 10 units; collision gas, N^2, (CAD), 2; nebulizer gas, N^2, 60 units; and auxiliary gas, N^2, 60 units. The two most abundant product ions for Largazole were *m/z* 497.1 and 357.1 and for Largazole thiol *m/z* 357.3 and 141.3. Samples were quantified by internal standard reference method in the MRM mode

monitoring ion transitions as indicated in Table 1. The dwell times for each ion transition were 100 ms Q_1 and Q_3 were both operated in unit resolution mode.

Quantitation of Largazole and Largazole thiol was based on the prepared standard curve of each respective compound using the ratio of either compounds summed peak areas to trazodone peak area and $1/x^2$ weighting of linear regression. Parameters for the assessment of assay performance were calculated as follows:

Pharmacokinetic Modeling

Serum concentrations were analyzed by noncompartmental and compartmental methods using a commercial software program (Phoenix® WinNonlin® v6.3, Pharsight Corporation, Mountain View, CA). Plasma concentration versus time curves were plotted on a semi-logarithmic graph to aid in selection of the most appropriate model for analysis. Serum concentration data were weighted by the reciprocal of the observed serum concentration squared. Models were compared for the most appropriate fit by observation of the residuals plot and using the goodness-of-fit criteria to select the best statistical model using Akaike's Information Criterion (AIC). The data were best fit by a two-compartment model described by the following equation: $C = A*e^{-\alpha t} + B*e^{-\beta t}$, where A and B are the intercepts for the rate constants of each phase. Noncompartmental parameters calculated included total body clearance (CL), volume of distribution at steady state (Vss), mean residence time (MRT), area-under-the-curve from time zero to infinity ($AUC_{0\text{-inf}}$) calculated using the linear trapezoidal method with linear interpolation, and area-under-the-first-moment-curve (AUMC).

Results

Macrocycle substitutions in Largazole are well tolerated

Several Largazole analogs as shown in Figure 1 were screened against colon (HT-116, HT-29, SW620), non-small cell lung carcinoma (A549), and pancreatic (MiaPaCa) cancer cell lines to determine growth inhibitory properties. As shown in Table 2A, all compounds tested inhibited growth with IC_{50}s in the mid to low nanomolar-high picomolar range. The pyridyl analog depsipeptide had very high potency as measured by IC_{50} that was more potent than the parent compound Largazole in all cell lines tested. Peptide isosteric replacement of the depsipeptide linkage was tolerable, however a loss of potency was observed (3–10 fold). The Largazole peptide isostere had levels of potency comparable to the pyridyl analog peptide isostere congener.

Analysis of IC_{50} inhibitory properties of Largazole and Largazole analogs against class I HDACs (HDAC 1,2,3) and the class IIb HDAC 6 is shown in Table 2A. Largazole and Largazole analogs were all more potent than the hydoxamate-based HDACi Vorinostat (SAHA) with Largazole, the pyridyl analog depsipeptide, and Largazole peptide isostere compounds having a potency that is at least 40–50 fold greater than Vorinostat to class I HDACs. Moreover selectivity to class I HDACs relative to HDAC 6 is ~30–160 for the pyridyl analog depsipeptide while the Largazole peptide isostere has a selectivity to class I HDACs that is ~170–340 fold relative to HDAC 6.

Induction of Apoptosis by Largazole Analogs

To further explore the potency of substituted macrocycle analogs of Largazole and their ability to induce an apoptotic response as measured by annexin V (AV) and propidium iodide (PI) staining was done in A549 cell lines at 24, 48 and 72 hours. As shown in Figure 2, all the compounds induced apoptosis as measured by annexin V staining in the low to mid-nanomolar range after 24 hours of drug exposure. Overall potency of the compounds followed the general trends observed in growth inhibition experiments, with the peptide isostere replacements requiring higher concentrations to achieve cell populations showing late (AV+/PI+) and early (AV+/PI−) apoptosis. A progression of apoptosis was shown in all compounds with the exception of the pyridyl analog peptide isostere. Notably, a sharp increase in the number of apoptotic cells was seen from 48 to 72 hours in the alternative prodrug Largazole analog, the pyridyl analog pyridyl disulfide. As shown in the micrographs above the raw cytometry data, striking cell morphology changes (spikes and blebs) that are the hallmark of apoptosis were evident within 24 hours post-treatment. Similar results were achieved in the SW620 and MIA PaCa cell lines (data not shown).

Cell Cycle Arrest by Largazole and Analogs

To evaluate changes in cell cycle distribution following treatment with Largazole and Largazole analogs, SW620 (colorectal adenocarcinoma) or A549 (non small cell lung carcinoma) cells were treated with the indicated concentrations of Largazole or analogs as shown in Figure 3 for 24 hours followed by propidium iodide staining and flow cytometry for cell cycle analysis. As shown in Figure 3 A-D, all compounds induced G1 arrest at low nanomolar concentrations (5–10 nM) relative to vehicle control in the SW620 cell line. As concentrations increased, a general trend towards G2 arrest was observed. An observation that is very similar to that reported by Luesh and co-workers (18). Largazole was particularly effective at G2 arrest at concentrations >50 nM with low peak CV for the G2 population indicating a uniform cell population. The peptide isotere analogs were not as effective at inducing G2 arrest, requiring concentrations >100 nM for G2 arrest. The pyridyl analog depsipeptide induced significant accumulation of the sub-G1 population (necrotic cells) at concentrations >10 nM (data not shown) as could be predicted based the IC_{50} potency measurements.

Interestingly, as shown in Figure 3E, no trend toward G2 arrest was seen in the A549 cell line at higher compound concentrations and cells remained arrested at G1/G0.

Method Development and Pharmacokinetic Modeling

Due to the rapid processing *in vivo* of the thioester prodrug structure of Largazole to the active thiol form, developing a bioanalytical method to analyze Largazole and prodrug proved challenging. Initial attempts to trap the active thiol with N-ethylmaleimide yielded fair results; however, poor precision and accuracy of measuring the prodrug in matrix led to the abandonment of this approach. In our method development studies, it was noted that processing of the prodrug was quite rapid and was < LLOQ after ten minutes of room temperature incubation in plasma or whole blood. Due to the risk of spurious results being generated during the processing of early time point samples, our solution was to focus solely

on the active thiol form of the drug. This was accomplished by the addition of a pre-extraction incubation in matrix to yield the thiol form of the drugs.

The second major obstacle encountered was the fact that the thiol form of Largazole forms adducts with blood components, presumably through thiol-disulfide exchange reactions. While developing the whole blood extraction protocol it was noted the addition of DTT improved recoveries of Largazole thiol by at least 30% therefore the final method includes a DTT reduction step to liberate, at least partially, adducted largazole thiol. While a full method validation was beyond the scope of our objectives, the range of the method was established as 1–1000 ng/mL for both Largazole thiol and Largazole peptide isostere thiol (data not shown). Samples expected to fall above the range were diluted 1:4 to ensure sufficient precision and accuracy. Quality Control (QC) samples processed during the LC-MS/MS analysis of the pharmacokinetic samples passed typical accuracy and precision acceptance criteria for a bioanalytical method and all QC samples were within ±15% the nominal value (data not shown).

As previously reported, the rationale for replacing the depsipeptide ester linkage present in Largazole with a peptide isostere linkage was to impart improved hydrolytic stability. To investigate if indeed the Largazole peptide isostere has improved pharmacokinetic properties relative to the parent natural product Largazole, female NIH Swiss mice were dosed via tail vein injection with 5 mg/kg Largazole or Largazole peptide isostere. Blood was collected at 5, 15, 30, 60, 120, and 240 minutes for analysis by LC-MS/MS. To model both the distribution phase and the elimination phase of Largazole and Largazole peptide isostere, a two-compartment model was chosen.

Upon inspection of the parameters of the two-compartment model shown in Table 3, it is clear that the two compounds' parameter estimates are quite similar. The two compounds have nearly identical distribution as signified by the similarities in V_{ss} as well as the volumes of the central (V1) and peripheral (V2) compartments (data not shown). The notable difference in drug exposure (AUC) observed between the two compounds, with the largazole peptide isostere showing an ~30% increase, is presumably due to the slower drug elimination, or stability. This increased drug exposure is manifested in the longer elimination half-life (Beta HL) as well as the decreased clearance (CL) and a longer mean residence time (MRT). Thus, Largazole and Largazole peptide isostere showed similar pharmacokinetic properties both with regards to drug distribution and drug elimination with the modest improvement in drug exposure unlikely to fully explain the difference of *in vivo* drug response.

It should be noted that tumor levels of the compounds were measured three hours after four consecutive days of treatment (pharmacodynamics, Figure 5) was also similar with measured levels of 215 24 ng/g and 141 32 ng/g for the largazole and largazole peptide isostere, respectively.

A549 Xenograft Model

To investigate the *in vivo* efficacy of Largazole and Largazole analogs, A549 non-small cell lung carcinoma cells were injected subcutaneous into the rear flank of aythimic nude mice.

Largazole or Largazole analogs were administered i.p. every other day at concentration of 5 mg/kg for thirteen days (seven total treatments). This dosage and schedule was chosen based on previously published values and to potentiate any pharmacokinetic advantage that may exist in Largazole peptide isostere analogs (18). As shown in Figure 4A, tumor growth rate was slower in Largazole, Largazole thiol, and Largazole peptide isostere treated mice compared with vehicle-treated controls. The results of the pair-wise, two-tailed Mann-Whitney test shown in Table 4 indicates that Largazole thiol and Largazole peptide isostere treated mice had tumor growth rate reductions that were statistically different from the control group ($p = 0.040$ and $p = 0.002$ respectively). Moreover, the Largazole peptide isostere was also statistically different from both Largazole and Largazole thiol ($p=0.006$ and $p=0.023$ respectively). Largazole was not statistically different from the control, likely due to the high standard deviation of tumor volumes within the group, however tumor growth inhibition (TGI%) was 32% of control. The TGI% for the Largazole thiol treated group was 42% and 66% for Largazole peptide isostere group relative to the control ten days after the last treatment (day 23). Surprisingly, neither pyridyl-substituted Largazole analog showed tumor growth inhibition in the A549 model using this every other day dosing regimen (data not shown), in spite of the high potency in cell-based assays for the pyridyl analog depsipeptide. The study was terminated at day 35 for humane reasons as no persistence of the treatment was observed.

Animal body condition was robust for the Largazole peptide isostere group with minimal weight loss occurring. As is clear from the TGI% of Largazole thiol, the masked the prodrug is fully dispensable for anti-tumor activity, a result that is not unexpected based on the rapid cleavage of the thioester-acyl tail in blood or plasma. On the other hand, mice in the Largazole thiol group experienced moderate weight loss (~2%) and one fatality occurred indicating that at least some toxicity may occur from use of the free thiol by this route of administration.

Phamcodynamics, Ki-67 IHC, and dose response In Vitro

To show engagement of HDAC therapeutic target *in vivo* previously treated xenograft animals were selected that were at endpoint (tumor volume 900–1000 mm^3 and >14 days since last dose) and were treated on four consecutive days with 5 mg/kg of Largazole compounds i.p. as discussed above. On day four animals were sacrificed three hours post-administration and tumors, blood, and organs were collected. As shown in Figure 5A, the Ki-67 marker for proliferation shows greatly reduced staining for Ki-67 in the Largazole, pyridyl analog desipeptide, and to a lesser degree in the Largazole peptide isostere tumor sections relative to the control. Only a slight difference in staining frequency/intensity was observed with the pyridyl analog peptide isostere and the pyridyl analog-pyridyl disulfide when compared to the control. As presented in Figure 5B an increase in acetylated H3 and H4 was observed in all samples relative to the control by western blot. Finally to demonstrate dose dependency of Largazole or Largazole analog treatment, A549 cells were treated with 10–1000 nM for 24 hours. All compounds generated an increase in acetylated H3 and H4 in a dose dependent fashion with levels of acetylation that parallels the observed potency of the compounds *in vitro* (Figure 5C)

Discussion

The work presented herein has shown that modification of the macrocycle and/or alternative prodrug structure of the highly potent class I selective marine natural product HDACi Largazole can be accomplished without loss of clinically exploitable activity. Indeed, the results of this study and our previous work reveals that desirable properties can be designed from the Largazole scaffold to achieve compounds that have improved clinical properties such as potency, class selectivity, and pharmacokinetics (16,17,19). As shown in Table 2B above, the Largazole peptide isostere is an exceptionally class I-selective HDACi relative to the parent depsipeptide natural product Largazole and may have unique clinical utility based on its highly selective HDACi profile.

Potency improvement has been demonstrated by decreased IC_{50}'s and induction of apoptosis as assessed by AV/PI staining observed for the pyridyl analog desipeptide particularly in the MIA PaCa cell line (data not shown). The potency of the pyridyl analog depsipeptide is at least that observed with clinically advanced hydroxamate HDACi Panobinostat in the cell lines tested here (7,20). Much to our surprise, the improved *in vitro* potency of this analog did not manifest in improved efficacy in the A549 xenograft model. The reason for this result is unknown at present and may be a result of poor pharmacokinetics or high-plasma protein binding with the pyridyl analog series. However, increasing dosing frequency to a daily regimen of the pyridyl analog depsipeptide did nearly abrogate Ki-67 IHC staining indicating a potential for better efficacy in future studies with higher dose levels or more frequent dosing.

The replacement of the relatively labile ester linkage of the depsipeptide found in the parent compound as well as Romidepsin (FK228) and Spiruchostatin can be predicted to improve hydrolytic stability (21). Indeed, the results of the two compartmental PK modeling suggest that this prediction held true *in vivo*. It is tempting to conclude that the modest improvements seen in clearance (CL) and AUC with the Largazole peptide isostere relative to the parent compound Largazole was the basis for the surprising efficacy observed in the xenograft work. However, reduced plasma protein binding, reduced affinity for p-glycoprotein (Pgp) or decreased up-regulation of *MDR1* may also play a role. Romipdesin has been shown to be a substrate for Pgp and its administration up-regulates *MDR1* expression and these observations are considered major factors in acquired resistance to Romidepsin (22,23). The level of tumor growth suppression observed in this study compares very favorably with other published studies of HDACi in the A549 xenograft model, further supporting the clinical importance of Largazole and Largazole analogs (7,24,25).

In summary, we have presented preclinical results on induction of apoptosis, cell cycle arrest, tumor growth suppression, and demonstrated the potential to modify the parent compound Largazole to improve *in vivo* performance. Further this work has shown the clinical importance of the marine HDACi Largazole and synthetic Largazole analogs that reveal the robust nature of the Largazole macrocycle scaffold to be used in future drug development programs. As we and others have shown, Largazole and its analogs are important clinical candidates and represent a promising new addition to the broad field of HDACi in clinical development.

Supplementary Material

Refer to Web version on PubMed Central for supplementary material.

Acknowledgements

This work was supported by the National Institutes of Health (RO1 CA152314, to RMW and JEB). JEB acknowledges support by grants from the National Cancer Institute (1K08CA128972) and the Burroughs-Wellcome Foundation (CAMS). JLP acknowledges support from the State of Colorado Bioscience Development Program Grant. This work was also supported by University of Colorado Cancer Center Shared Resource (Pharmacology) support grant (P30CA046934).

Financial Support: This work was supported by the National Institutes of Health (RO1 CA152314, to RMW and JEB). JEB acknowledges support by grants from the National Cancer Institute (1K08CA128972) and the Burroughs-Wellcome Foundation (CAMS). JLP acknowledges support from the State of Colorado Bioscience Development Program Grant. This work was also supported by University of Colorado Cancer Center Shared Resource (Pharmacology) support grant (P30CA046934).

Literature Cited

1. Wagner JM, Hackanson B, Lübbert M, Jung M. Histone deacetylase (HDAC) inhibitors in recent clinical trials for cancer therapy. Clin Epigenetics. 1:117–136. [PubMed: 21258646]
2. Woo S, Gardner ER, Chen X, Ockers SB, Baum CE, Sissung TM, et al. Population pharmacokinetics of romidepsin in patients with cutaneous T-cell lymphoma and relapsed peripheral T-cell lymphoma. Clin Cancer Res. 15:1496–1503. [PubMed: 19228751]
3. Subramanian S, Bates SE, Wright JJ, Espinoza-Delgado I, Piekarz RL. Clinical Toxicities of Histone Deacetylase Inhibitors. Pharmaceuticals. 3:2751–2767.
4. Ververis K, Hiong A, Karagiannis TC, Licciardi P V. Histone deacetylase inhibitors (HDACIs): multitargeted anticancer agents. Biologics. 7:47–60. [PubMed: 23459471]
5. Lobera M, Madauss KP, Pohlhaus DT, Wright QG, Trocha M, Schmidt DR, et al. Selective class IIa histone deacetylase inhibition via a nonchelating zinc-binding group. Nat Chem Biol. 9:319–325. [PubMed: 23524983]
6. Marks PA. Discovery and development of SAHA as an anticancer agent. Oncogene. 26:1351–1356. [PubMed: 17322921]
7. Crisanti MC, Wallace AF, Kapoor V, Vandermeers F, Dowling ML, Pereira LP, et al. The HDAC inhibitor panobinostat (LBH589) inhibits mesothelioma and lung cancer cells in vitro and in vivo with particular efficacy for small cell lung cancer. Mol Cancer Ther. 8:2221–2231. [PubMed: 19671764]
8. Richardson PG, Schlossman RL, Alsina M, Weber DM, Coutre SE, Gasparetto C, et al. PANORAMA 2: panobinostat in combination with bortezomib and dexamethasone in patients with relapsed and bortezomib-refractory myeloma. Blood. 122:2331–2337. [PubMed: 23950178]
9. Bradner JE, West N, Grachan ML, Greenberg EF, Haggarty SJ, Warnow T, et al. Chemical Phylogenetics of Histone Deacetylases. Nat Chem Biol. 2010; 6:238–243. [PubMed: 20139990]
10. Khan N, Jeffers M, Kumar S, Hackett C, Boldog F, Khramtsov N, et al. Determination of the class and isoform selectivity of small-molecule histone deacetylase inhibitors. Biochem J. 409:581–589. [PubMed: 17868033]
11. Taori K, Paul V, Luesch H. Structure and Activity of Largazole, a Potent Antiproliferative Agent from the Floridian Marine Cyanobacterium Symploca sp. J Am Chem Soc. 2008; 130:1806–1807. [PubMed: 18205365]
12. Bowers A, West N, Taunton J, Schreiber SL, Bradner JE, Williams RM. Total synthesis and biological mode of action of largazole: a potent class I histone deacetylase inhibitor. J Am Chem Soc. 130:11219–11222. [PubMed: 18642817]
13. Ying Y, Taori K, Kim H, Hong J. Total Synthesis and Molecular Target of Largazole, a. Histone. 2008; 4:1–5.

14. Benelkebir H, Marie S, Hayden AL, Lyle J, Loadman PM, Crabb SJ, et al. Total synthesis of largazole and analogues: HDAC inhibition, antiproliferative activity and metabolic stability. Bioorg Med Chem. 19:3650–3658. [PubMed: 21420302]
15. Cole KE, Dowling DP, Boone MA, Phillips AJ, Christianson DW. Structural Basis of the Antiproliferative Activity of Largazole, a Depsipeotide Inhibitor of the Histone Deacetylases. J Am Chem Soc. 2011; 133:12474–12477. [PubMed: 21790156]
16. Bowers AA, Greshock TJ, West N, Estiu G, Stuart L, Wiest O, et al. Synthesis and Conformation-Activity Relationships of the Peptide Isosteres of FK228 and Largazole. J Am Chem Soc. 2009; 131:2900–2905. [PubMed: 19193120]
17. Bowers AA, West N, Newkirk TL, Troutman-youngman AE, Schreiber SL, Wiest O, et al. Synthesis and HDAC Inhibitory Activity of Largazole Analogs: Alteration of the Zinc-Binding Domain and Macrocyclic Scaffold. Org Lett. 2009; 11:1301–1304. [PubMed: 19239241]
18. Liu Y, Salvador LA, Byeon S, Ying Y, Kwan JC, Law BK, et al. Anticolon Cancer Activity of Largazole , a Marine-Derived Tunable Histone Deacetylase Inhibitor. J Pharmacol Exp Ther. 2010; 335:351–361. [PubMed: 20739454]
19. Guerra-Bubb JM, Bowers A a, Smith WB, Paranal R, Estiu G, Wiest O, et al. Synthesis and HDAC inhibitory activity of isosteric thiazoline-oxazole largazole analogs. Bioorg Med Chem. 23:6025–6028.
20. Labonte MJ, Wilson PM, Fazzone W, Russell J, Louie SG, El-khoueiry A, et al. The dual EGFR/HER2 inhibitor lapatinib synergistically enhances the antitumor activity of the histone deacetylase inhibitor panobinostat in colorectal cancer models. Cancer Res. 2012; 71:3635–3648. [PubMed: 21464044]
21. Nassar A-EF, Kamel AM, Clarimont C. Improving the decision-making process in the structural modification of drug candidates: enhancing metabolic stability. Drug Discov Today. 9:1020–1028. [PubMed: 15574318]
22. Robey RW, Zhan Z, Piekarz RL, Kayastha GL, Fojo T, Bates SE. Increased MDR1 expression in normal and malignant peripheral blood mononuclear cells obtained from patients receiving depsipeptide (FR901228, FK228, NSC630176). Clin Cancer Re. 2006; 12:1547–1555.
23. Xiao JJ, Foraker AB, Swaan PW, Liu S, Huang Y, Dai Z, et al. Efflux of Depsipeptide FK228 (FR901228, NSC-630176) Is Mediated by P-Glycoprotein and Multidrug Resistance- Associated Protein 1. J Pharmacol Exp Ther. 2005; 313:268–276. [PubMed: 15634944]
24. Beckers T, Burkhardt C, Wieland H, Gimmnich P, Ciossek T, Maier T, et al. Distinct pharmacological properties of second generation HDAC inhibitors with the benzamide or hydroxamate head group. Int J Cancer. 121:1138–1148. A. [PubMed: 17455259]
25. Fournel M, Bonfils C, Hou Y, Yan PT, Trachy-Bourget M-C, Kalita A, et al. MGCD0103, a novel isotype-selective histone deacetylase inhibitor, has broad spectrum antitumor activity in vitro and in vivo. Mol Cancer Ther. 7:759–768. [PubMed: 18413790]

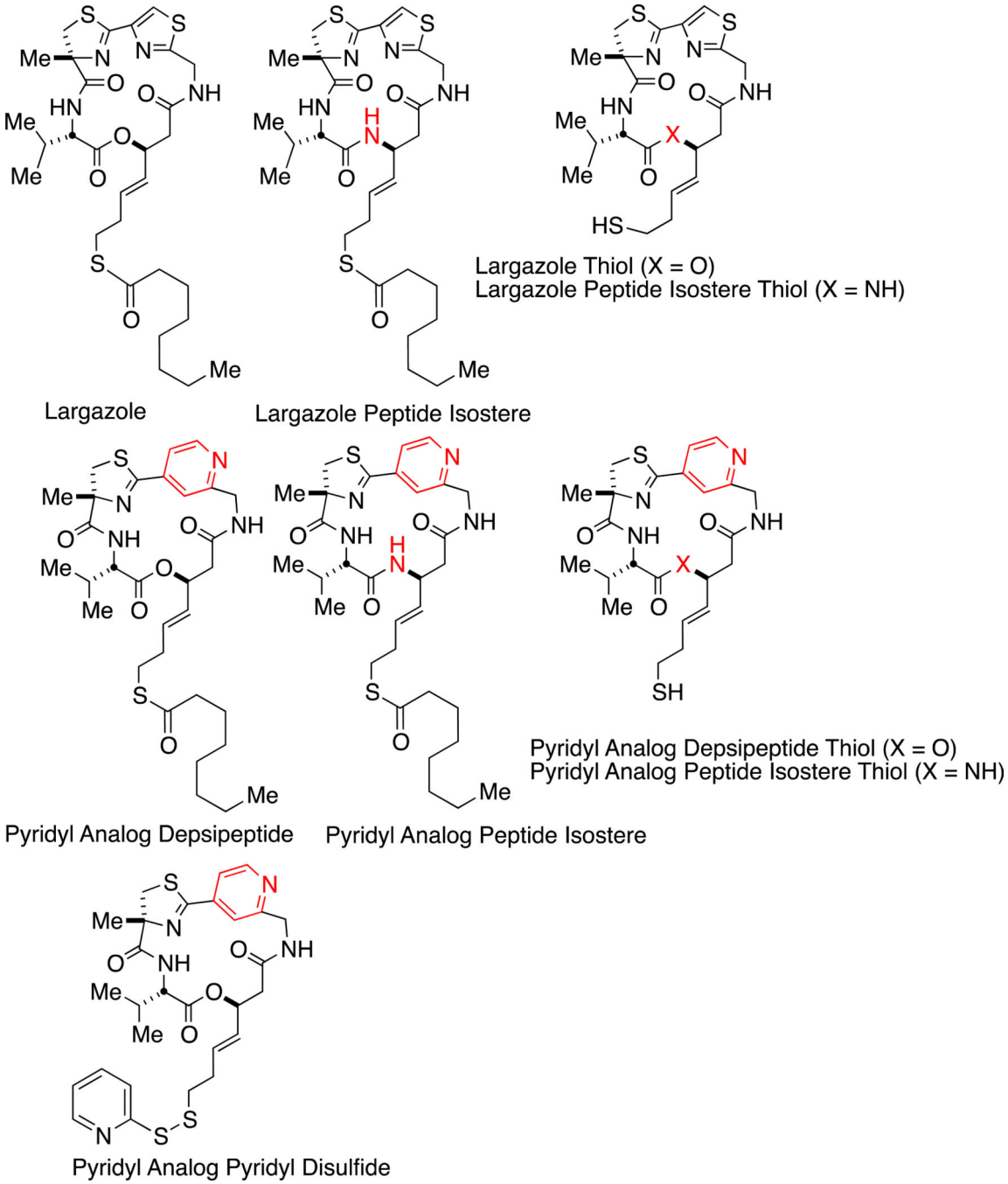

Figure 1.

Structures of compounds used in this study. Marcrocycle analogs of Largazole were synthesized to replace the thiazole in the parent compound Largazole with a pyridyl group, to substitute a peptide isostere for the depsipeptide, and to replace the thioester prodrug with a pyridyl-disulfide.

A

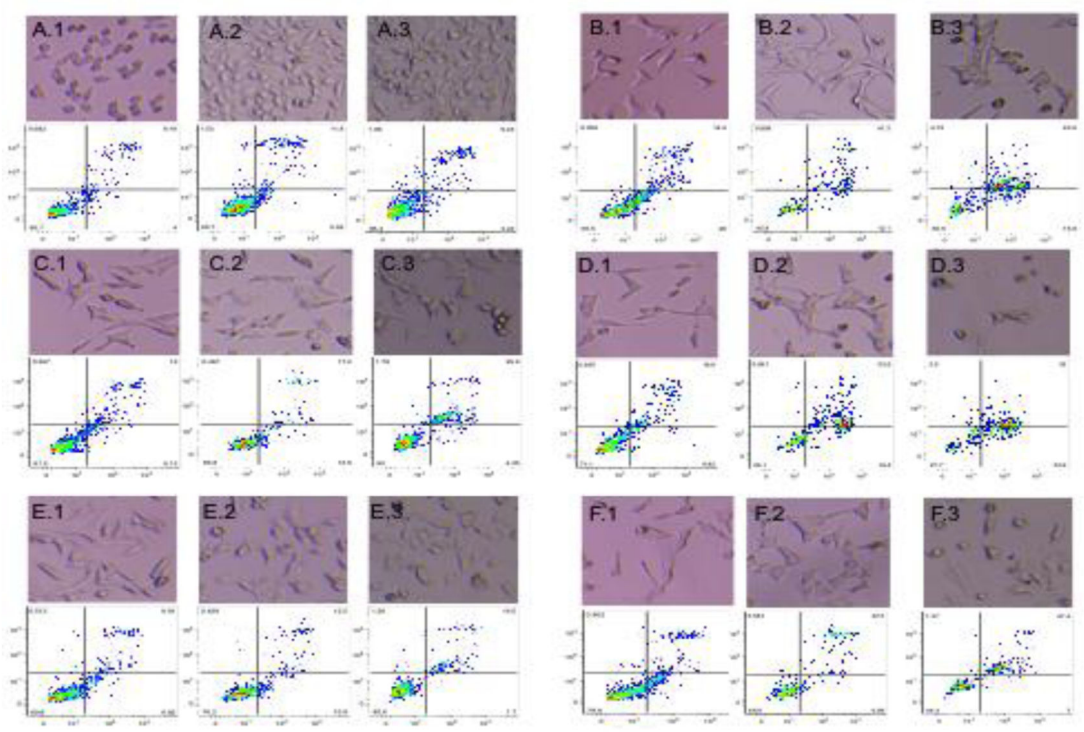

B

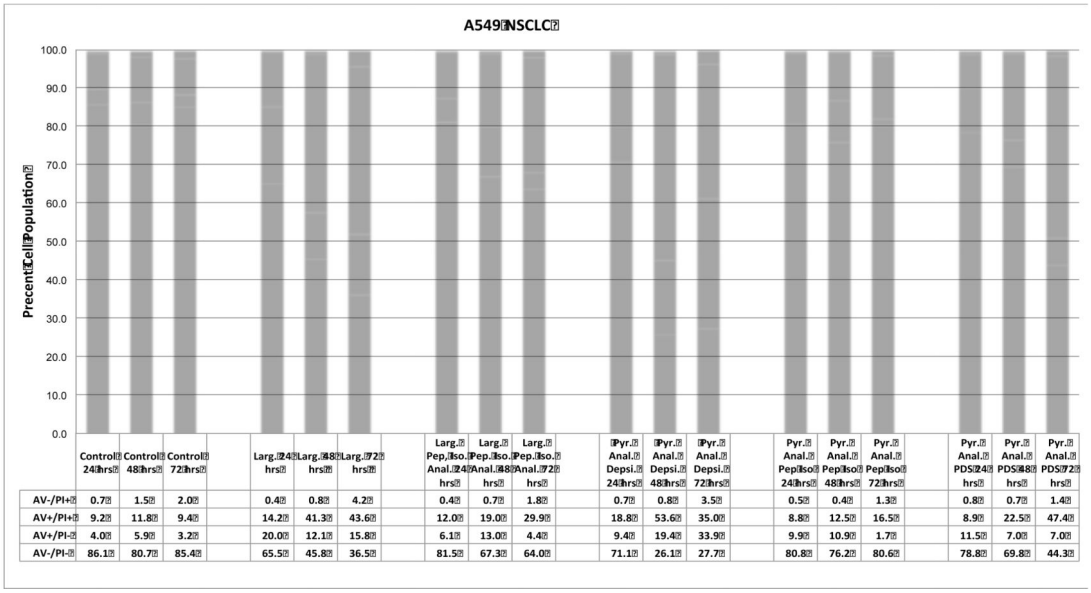

	Control 24hrs	Control 48hrs	Control 72hrs	Larg. 24 hrs	Larg. 48 hrs	Larg. 72 hrs	Larg. Pep, Iso. Anal. 24 hrs	Larg. Pep. Iso. Anal. 48 hrs	Larg. Pep. Iso. Anal. 72 hrs	Pyr. Anal. Depsi. 24hrs	Pyr. Anal. Depsi. 48hrs	Pyr. Anal. Depsi. 72hrs	Pyr. Anal. Pep Iso 24hrs	Pyr. Anal. Pep Iso 48hrs	Pyr. Anal. Pep Iso 72hrs	Pyr. Anal. PDS 24 hrs	Pyr. Anal. PDS 48 hrs	Pyr. Anal. PDS 72 hrs
AV-/PI+	0.7	1.5	2.0	0.4	0.8	4.2	0.4	0.7	1.8	0.7	0.8	3.5	0.5	0.4	1.3	0.8	0.7	1.4
AV+/PI+	9.2	11.8	9.4	14.2	41.3	43.6	12.0	19.0	29.9	18.8	53.6	35.0	8.8	12.5	16.5	8.9	22.5	47.4
AV+/PI-	4.0	5.9	3.2	20.0	12.1	15.8	6.1	13.0	4.4	9.4	19.4	33.9	9.9	10.9	1.7	11.5	7.0	7.0
AV-/PI-	86.1	80.7	85.4	65.5	45.8	36.5	81.5	67.3	64.0	71.1	26.1	27.7	80.8	76.2	80.6	78.8	69.8	44.3

Figure 2.

(A) Assessment of apoptosis of A549 cells at 24 (X.1),48 (X.2), and 72 (X.3) hours by Annexin V and cell morphology changes and **(B)** graphical representation of Annexin V and propidium iodide staining. A549 cells were incubated in the presence of 150 nM Largazole (B.1-B.3), 300 nM Largazole peptide isostere (C.1-C-3),150 nM pyridyl analog depsipeptide (D.1-D.3), 300 nM pyridyl analog peptide isostere (E.1-E.3) and 300 nM pyridyl analog-pyridyl disulfide (F.1-F.3) and compared to control (A.1-A.3). Cell morphology changes indicative of apoptosis (spikes and blebs) are shown above the corresponding raw cytometry

data. Lower panel **B** presents the cell percentage of cells undergoing an apoptotic response (AV+/PI-), green and AV+/PI+, red).

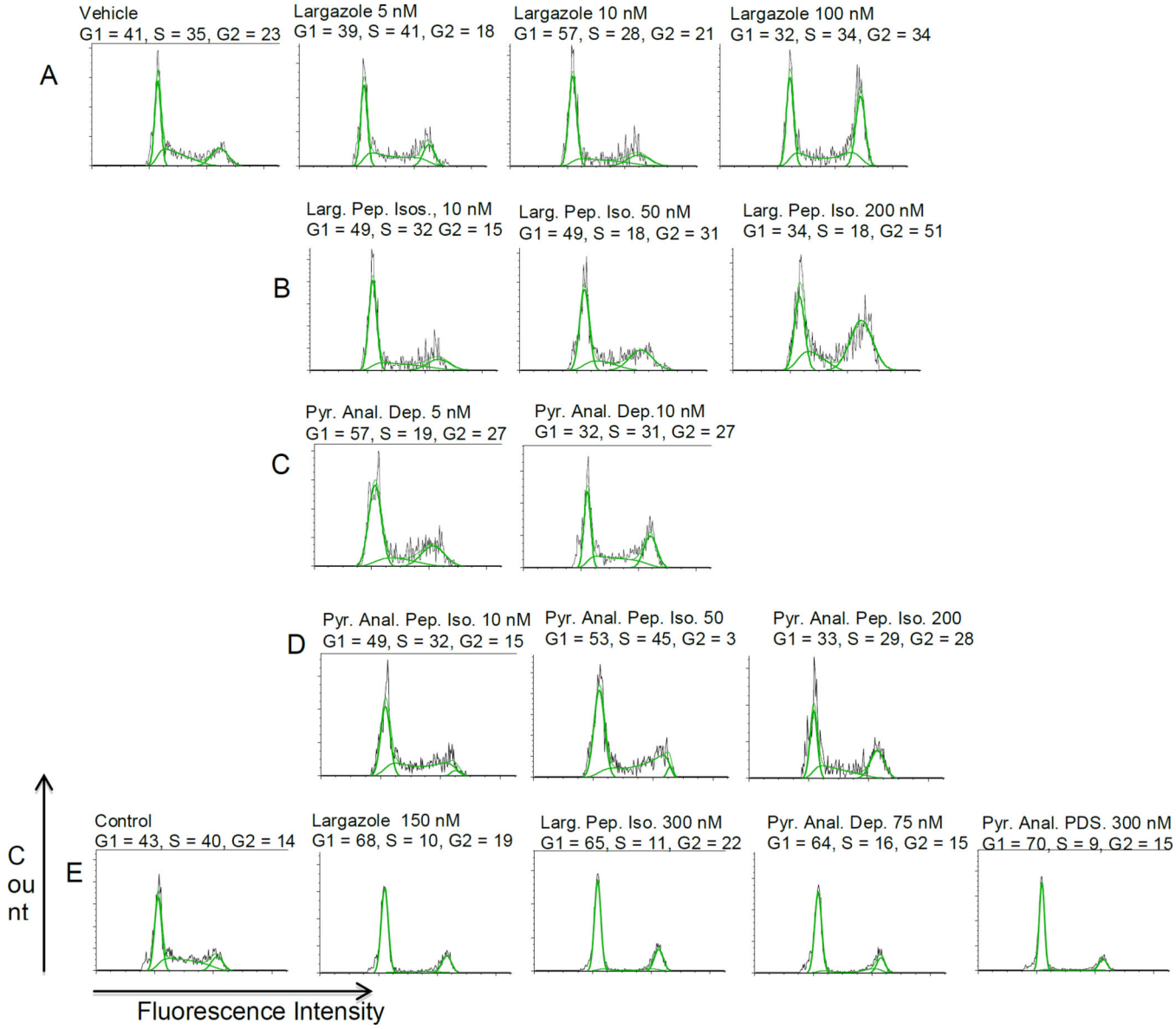

Figure 3.

(A-D) dose dependence on cell cycle in colorectal cell line SW620 and (**E**), in A549 non-small cell lung carcinoma cells. In the SW620 cell line there is a clear switch from G1 to G2 arrest with increasing concentration, particularly for largazole and largazole isostere, this was not observed to occur in the A549 non-small cell lung carcinoma line and cells remained arrested in G1.

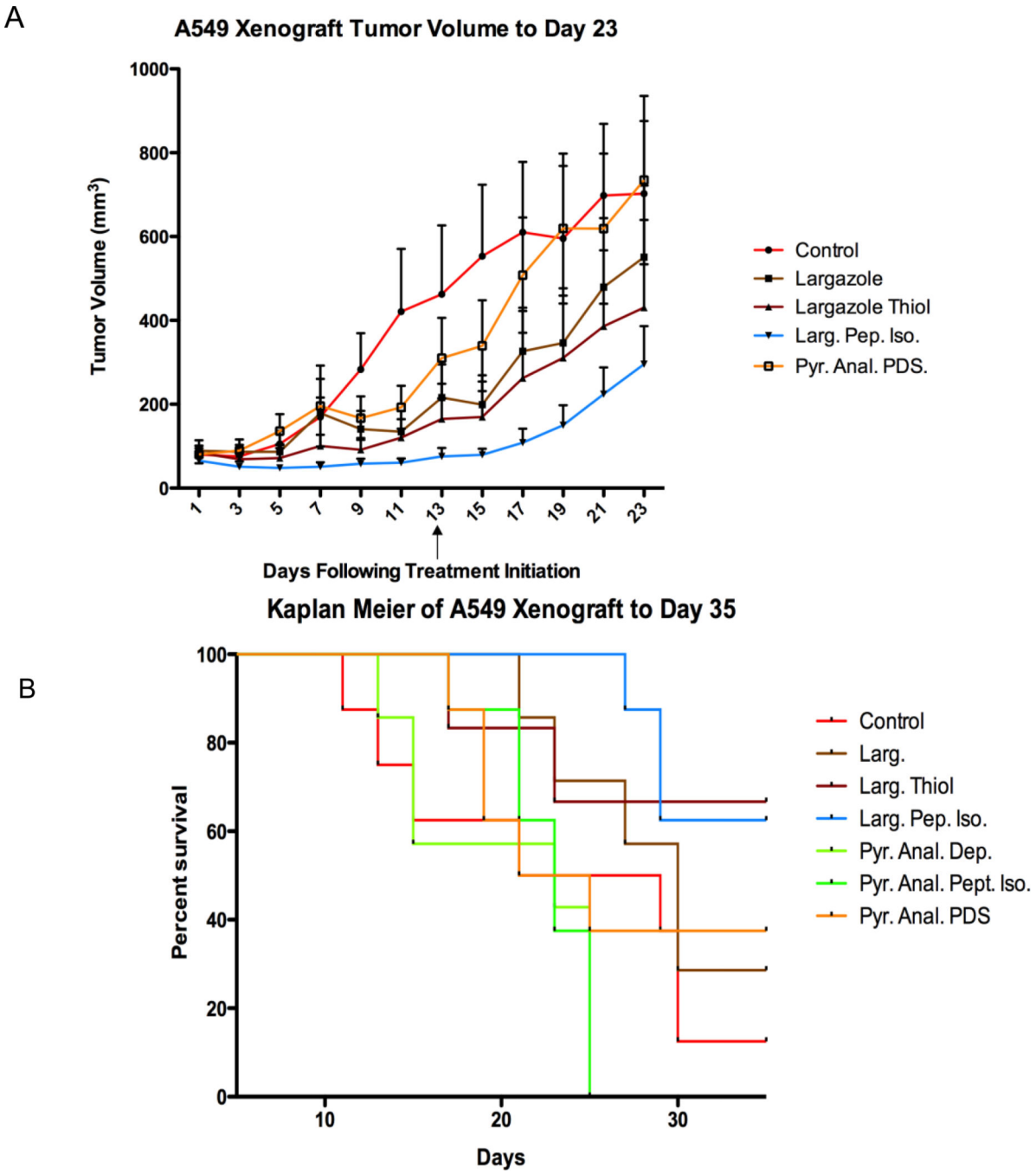

Figure 4.

(A) Tumor growth inhibition curve, **(B)** overall survivorship. Tumor growth profile to day 23 is shown in **a** the final treatment day is marked with an arrow. Tumor volumes increased more rapidly following cessation of treatment. Kaplan Meier curves to end of study (day 35) are shown in **B**.

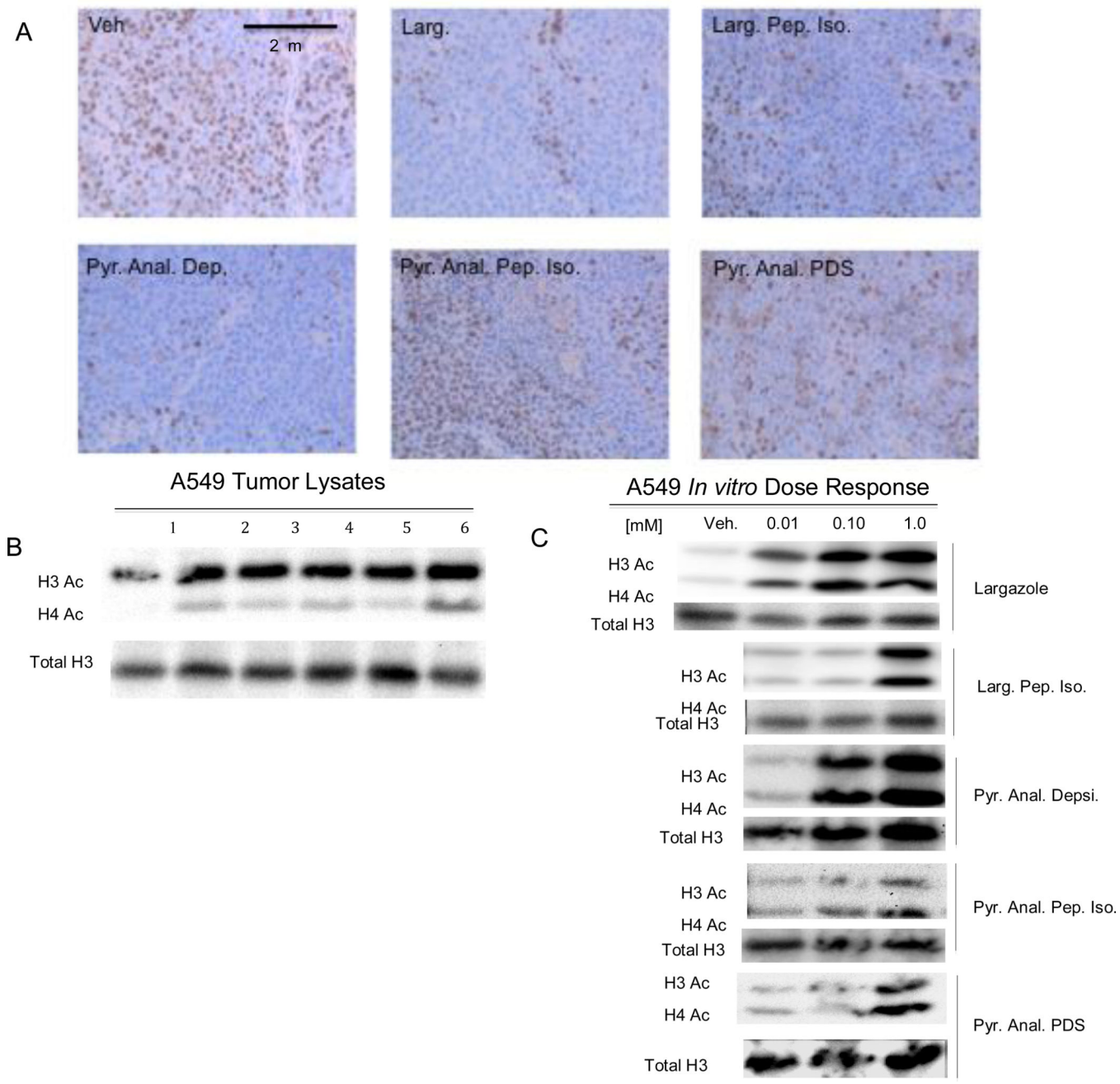

Figure 5.

(A) Immunohistochemistry of the proliferation marker Ki-67 in A549 tumor sections, **(B)** western blot of tumor lysate probed for acetylated H3 and H4, **(C)** western blot of A549 cells treated with Largazole or Largazole analogs. Staining for the Ki-67 proliferative marker **(A)** in tumor sections is greatly decreased relatively to control in the pyridyl analog depsipeptide, Largazole peptide isostere, and decreased moderately in the pyridyl analog pyridyl disulfide treatment. Western blots of tumor lysates **(B)** probed with anti-acetylated H3 and H4 show increased acetylation relative to control for all compounds (lane 1 control, lane 2 Largazole, lane 3 Largazole peptide isostere, lane 4 pyridyl analog depsipeptide, lane

5 pyridyl analog peptide isostere, lane 6 pyridyl analog pyridyl disulfide). Dose response of histone acetylation **(C)** *in vitro*.

Table 1

Optimized mass spectrometer settings for Largazole, Largazole thiol and Trazodone (IS).

Compound	MRM (m/z → m/z)	DP	EP	CEP	CE	CXP
Largazole	623.2 → 497.1	50.02	6.57	34.16	31.02	4.42
	623.2 → 357.1	50.4	5.73	109.92	42.40	5.2
Largazole thiol	497.0 → 357.3	46.2	4.20	63.13	32.1	5.4
	497.0 → 141.3	58.0	3.86	84.16	33.02	4.35
Trazodone	372.2 → 176.1	56.86	4.08	20.56	32.75	2.72

A. Calculated IC_{50} (nM) of Largazole and Largazole Analogs in Select Cell Lines

Compound	HTC-116	HT-29	SW620	A549	MiaPaCa
Largazole	3.5	16.2	26.5	3.8	206.4
Largazole Peptide Isostere	103.3	81.0	224.8	281.2	842.7
Pyridyl Analog Depsipeptide	0.7	0.3	8.2	0.18	91.8
Pyridyl Analog Peptide Isostere	82.9	31.5	81.0	542.7	3536
Pyridyl Analog Pyridyl Disulfide	ND	ND	ND	719.4	3290

B. Calculated Inhibitory IC_{50} (nM) of Largazole and Largazole Analogs Verses HDAC 1,2,3,6*

Compound	HDAC 1	HDAC 2	HDAC 3	HDAC 6
Largazole Thiol	3.4	10.5	10.4	203.6
Largazole Peptide Isostere Thiol	5.8	10.0	12.0	2045
Pyridyl Analog Depsipeptide Thiol	3.9	16.5	17.9	654.5
Pyridyl Analog Peptide Isostere Thiol	38.7	76.4	82.8	33710
Pyridyl Analog Pyridyl Disulfide	ND	ND	ND	ND
Vorinostat (SAHA)	136.7	211.5	206.9	143.4

* ND = not determined

* All compounds tested were the unmasked thiol forms.

Table 3

Two compartmental Model Parameters (Largazole vs. Largazole Peptide Isostere)

Parameter	Units	Largazole	Larg. Pep. Iso.	% Difference
C_{max}	µg/ml	5.4	4.8	12.5%
AUC	min*µg/mL	31.34	44.69	−29.9%
Alpha	1/min	0.336	0.248	35.5%
Beta	1/min	0.006	0.005	20.0%
Alpha HL	min	2.06	2.80	−26.4%
Beta HL	min	116	139	−16.5%
CL	mL/min/kg	160	111	44.1%
MRT	min	84	108	−22.2%
Vss	L/kg	13.45	12.10	11.1%

Table 4

P Values* and TGI% at Day 23

	Larg.	Larg. Thiol	Larg. Pep. Iso
Control	0.175	0.040	0.002
Larg.	-	0.446	0.006
Larg Thiol	-	-	0.023
TGI %	32%	42%	66%

* *p* values determined by Mann Whitney t-test